A bistable structural element

T Schioler[1] and **S Pellegrino**[2*]
[1]ITER Organization, Cadarache, St Paul-lez-Durance, France
[2]Graduate Aeronautical Laboratories, California Institute of Technology, Pasadena, California, USA

The manuscript was received on 15 December 2007 and was accepted after revision for publication on 30 April 2008.

DOI: 10.1243/09544062JMES982

Abstract: This article presents a novel bistable structural element that has high stiffness in stable configurations, but requires only a small amount of energy to be switched from one configuration to the other. The element is based on a planar linkage of four bars connected by revolute joints, braced by tape-spring diagonals. A description of the concept is presented, along with a detailed theoretical analysis of its mechanical behaviour. Experimental measurements obtained from a prototype structure are found to be in very good agreement with the predictions from this analytical model.

Keywords: adaptive structure, variable geometry structure, truss

1 INTRODUCTION AND BACKGROUND

Most structures are intended to be operational only in the shape in which they are constructed, but there is also a category of structures – often described as reconfigurable or adaptive – that are required to change their configuration during normal use. Reconfigurable structures surround us in our everyday lives; examples include robotic manipulators, desk lamps, and so on.

An important class of structures with a variable configuration, known as variable geometry trusses (VGTs), has been extensively investigated in the context of crane-like manipulators to build large space stations or exploration vehicles in orbit [1–4]. A VGT is a three-dimensional assembly of struts connected by spherical joints. Its configuration is uniquely determined by the length of the struts, through the choice of kinematically determinate architectures. Also, statically determinate architectures are adopted in order to ensure that any change in the length of the struts is accommodated purely by a change in the geometry, without inducing internal stresses in the structure. In other words, the structure does not fight against the imposed change in the length of the strut [5]. A simple two-dimensional example with a single bistable element is shown in Fig. 1; a structure with n bistable elements has 2^n unique configurations [6].

In the late 1960s, a new type of reconfigurable structure was proposed by Leifer and Scheinman, who were developing working models for the Stanford Artificial Intelligence Project. The concept, first published by Pieper in 1968 [7], envisaged manipulator joints with a finite number of discrete configurations. The argument for reducing the freedom of motion of the joints was that it would be much easier to integrate the manipulator with the digital computers that would control it. This approach was later extended to complex structures, such as VGTs, by Chirikjian and co-workers [8–10], using pneumatic actuators as structural elements capable of adopting two different lengths. Extensive studies of the kinematics, both direct and inverse, of structures containing elements that can adopt only a number of discrete configurations have been published [8, 10–13]. However, little work has been done on the components from which such structures may be manufactured. Also, there are still no mature actuator technologies that can be readily integrated into such components.

The research presented in this article was motivated by the need to provide bistable structural elements that may be coupled with the electrostrictive polymer artificial muscles actuators that have been developed in the Field and Space Robotics Laboratory at MIT [11, 12].

This article presents a novel bistable structural element that provides high stiffness in both stable states,

*Corresponding author: Graduate Aeronautical Laboratories, California Institute of Technology, 1200 E. California Boulevard, MC 301-46, Pasadena, CA 91125, USA. email: sergiop@caltech.edu

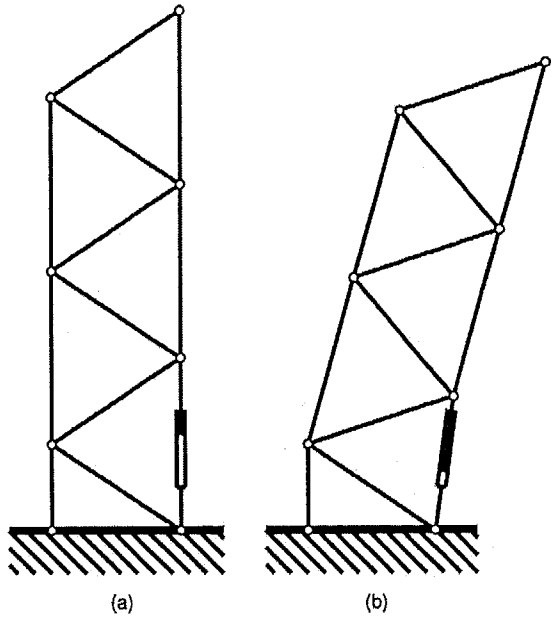

Fig. 1 Sketch of a two-dimensional VGT with a single bistable element (a) element extended and (b) element shortened by 20 per cent

but requires only a small amount of energy to be switched from one stable configuration to the other. This novel element is based on a planar linkage of four bars connected by revolute joints, braced by tape-spring diagonals. A detailed description of the concept, of which two prototypes have been made, will be presented along with a theoretical analysis and experimental results obtained from one of the prototypes. The coupling between structural elements and actuators has been investigated elsewhere [14].

The layout of the article is as follows. The next section describes the proposed bistable structural element. Section 3 presents a general analysis of the force versus length relationship of this element. Section 4 describes detailed predictions for a specific design of the element. A methodology for the design of bistable elements is proposed in section 5. A parametric design study is carried out for one particular type of tape spring element that are commercially available and choosing the minimal number of tape springs. Section 6 concludes the paper.

2 CONCEPT DESCRIPTION

The structural element is shown in Figs 2 and 3. It consists of four bars of equal length, connected by revolute joints with parallel axes, and two tape springs [15], connecting pairs of diagonally opposite joints of the four-bar mechanism. A tape spring is a thin cylindrical shell whose cross-section forms a circular arc of

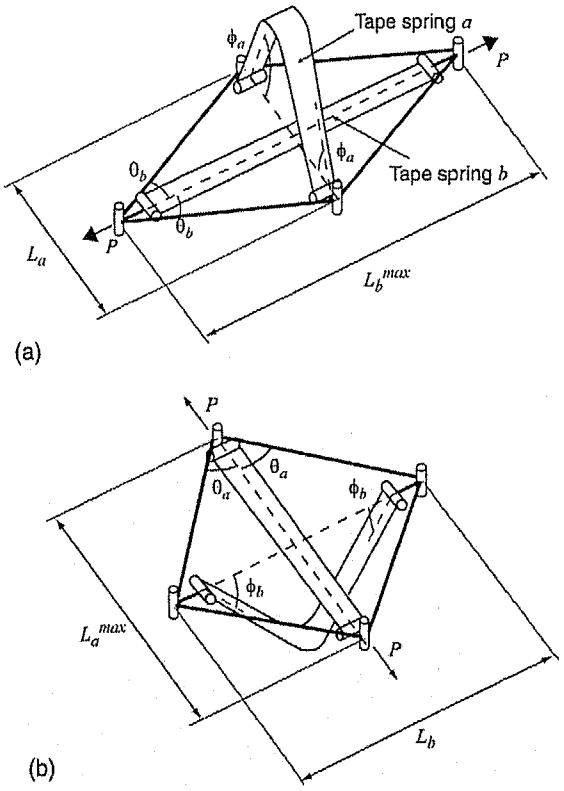

Fig. 2 Schematic diagram of the bistable structural element

uniform radius. The joints between the tape springs and the bars constrain only the rotation of the tape spring about its longitudinal axis.

The geometry of the linkage makes it impossible for both tape springs to be straight (unbuckled) at the same time. When a tape spring is buckled, it exerts a relatively small force on the four-bar linkage. This force is considerably lower than that required to buckle the other, straight tape spring. As a result, the element is stable and stiff when one tape spring or the other is

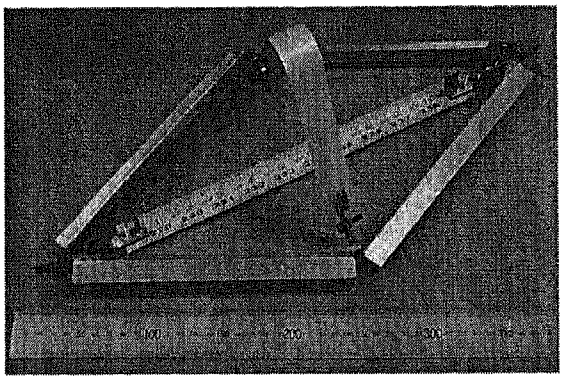

Fig. 3 First prototype

straight. The element has relatively low stiffness when both tape springs are buckled.

The angles between the tape springs and the plane of the linkage are denoted by ϕ_a and ϕ_b; the semi-angles between the bars of the linkage are denoted by θ_a and θ_b.

3 ANALYSIS

This structure can be analysed in three steps. The first step considers a single tape spring in a buckled state. The second step considers a tape spring in a non-buckled state. The final step combines the results of the first two steps with the geometry of the linkage to obtain the overall force–displacement relationship of the structure.

Step 1: Forces applied by a buckled tape spring. The bending moment in the uniform radius elastic fold at the centre of a buckled tape spring remains constant over a wide range of end rotations [**15, 16**]. Depending on whether the buckling of the tape spring involves bending in the sense opposite to that of the cross-section, in which case the longitudinal edges are in tension, or in the same sense as the cross-section, in which case the longitudinal edges are in compression, the magnitudes of the respective moments are

$$M_+^* = (1+\nu)D\alpha \quad \text{or} \quad M_-^* = (1-\nu)D\alpha \tag{1}$$

where

$$D = \frac{Et^3}{12(1-\nu^2)} \tag{2}$$

where α is the angle subtended by the cross-section of the tape spring and t its thickness. E and ν are the Young's modulus and Poisson's ratio, respectively.

Once M_+^* and M_-^* are known, it is possible to calculate the forces exerted by each tape spring on the four-bar linkage. Figure 4 shows the geometry of tape spring a when it is in a buckled state. Knowing the moment exerted by the tape spring, M_+^* or M_-^*, the length of the tape spring, S_a, and the longitudinal radius of curvature of the elastic fold region of the tape spring, R, the force F_a is given by

$$F_a = \frac{M^*}{[(S_a/2) - \phi_a R]\sin\phi_a + R(1-\cos\phi_a)} \tag{3}$$

Similarly, for tape spring b

$$F_b = \frac{M^*}{[(S_b/2) - \phi_b R]\sin\phi_b + R(1-\cos\phi_b)} \tag{4}$$

Note that the longitudinal radius of the elastic fold, R, in an isotropic tape spring is equal to the radius of the cross-section, r, [**16**], therefore

$$R = r \tag{5}$$

Step 2: Critical load of the unbuckled tape spring. Here the analysis given in reference [**17**] is followed. If the tape spring is long, the critical value of the axial force (i.e. the axial load at which the tape spring buckles), F_{cr}, can be predicted using the Euler buckling formula

$$F_{cr} = F_E = \frac{\pi^2 EI}{S^2} \tag{6}$$

where S is either S_a or S_b and I is the (minor) second moment of area of the cross-section of the tape spring.

However, this formula does not produce accurate predictions for the relatively short lengths of the tape spring which are of interest in this study. This is because the critical load is governed by the local buckling of the shell rather than the global buckling of the tape spring.

A more accurate analysis, shown next, takes this into account by considering the critical stress at points 1 and 2 of the tape spring, as shown in Fig. 5. The tape spring consists of two flat edge regions surrounding a central cylindrical region (for more details, see Fig. 8); hence, point 1 lies on the edge of a flat plate, whereas point 2 lies in a cylindrical panel. Therefore, the critical stress at each point is calculated as follows.

Point 1: Here, the tape spring is flat. Reference [**18**] gives the following expression for the critical stress in

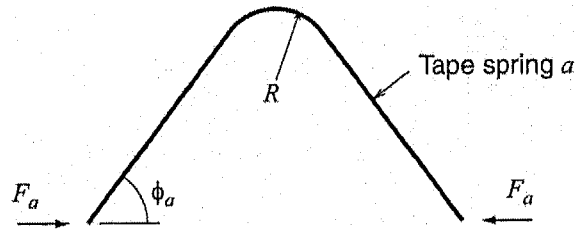

Fig. 4 Side view of tape spring a in the buckled configuration

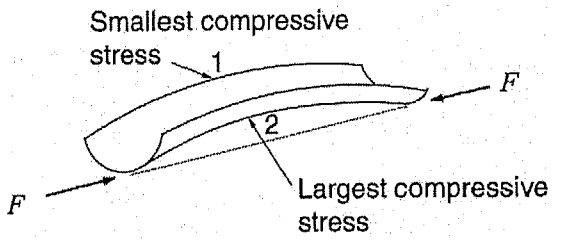

Fig. 5 Stresses in the tape spring that is on the point of buckling

a rectangular plate of width b

$$\sigma_{cr1} = \frac{k\pi^2 E}{12(1-\nu^2)}\left(\frac{t}{b}\right)^2 \tag{7}$$

where k is a constant that depends on the boundary conditions (Fig. 9).

Point 2: Here, the tape spring can be considered as a cylindrical panel. The buckling load for a cylindrical panel is given by Timoshenko and Gere [19]

$$\sigma_{cr2} = 0.6\frac{Et}{r} \tag{8}$$

Having determined the critical stresses at points 1 and 2, the actual stresses at those points for a given load should be calculated. In general, the stress at any point in an eccentrically loaded beam can be found from

$$\sigma = F\left(\frac{1}{A} + \frac{wy}{I}\right) \tag{9}$$

where y is the distance of the point of interest from the centroid and w is the eccentricity of the load from the centroid, as shown in Fig. 6.

The deflected shape of the tape spring also needs to be taken into account. The central deflection w of an eccentrically loaded strut, as shown in Fig. 6, is given in reference [20]

$$w = e\sec\left(\frac{\pi}{2}\sqrt{\frac{F}{FE}}\right) = \frac{e}{\cos\sqrt{FS^2/4EI}} \tag{10}$$

where e is the offset of the loading point from the centroid in the unloaded configuration.

Whether the critical stress is first reached at point 1 or point 2 depends on the value of e. The calculation is analogous for the two points; therefore, details are provided for one case only. Calculating F_{cr} for point 2 involves combining equations (9) and (10); this gives

$$\sigma_{cr2} = F_{cr}\left(\frac{1}{A} + \frac{e^2}{I\cos\sqrt{F_{cr}S^2/(4EI)}}\right) \tag{11}$$

As σ_{cr2} is given by equation (8), the only unknown in this equation is F_{cr}.

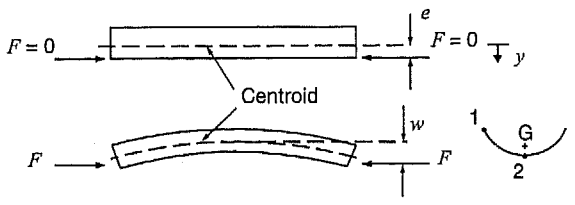

Fig. 6 Definition of eccentricity w

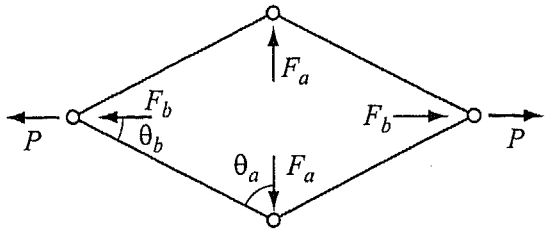

Fig. 7 Free body diagram for four-bar linkage

Step 3: Combination of results. Each of the two tape springs is connected to the four-bar linkage; a free body diagram is shown in Fig. 7.

Once the characteristics of the individual tape springs have been established, it is possible to calculate P by analysing the free body diagram shown in Fig. 7. The outcome is

$$P = -F_b + \frac{F_a}{\tan\theta_b} \tag{12}$$

Using equation (12), one can predict the variation of P with L_b. In the configurations where the tape springs are buckled, F_a and F_b are given by equations (3) and (4), respectively. When loaded in tension, the tape springs can be assumed to behave as linear-elastic axial elements.

4 RESULTS

The dimensions of the first prototype are listed in Table 1. The tape springs (Fig. 3) were cut from 'contractor grade' tape-measures supplied by Sears Roebuck and Co. Their cross-sectional shape and dimensions are given in Fig. 8. Note that only the central part is curved and the edges are flat. The second

Table 1 Dimensions of the first prototype

Dimension	Value
$S_a = S_b$ (mm)	372
e_a, e_b (mm)	−2.5
A (mm^2)	2.55
B (mm)	208

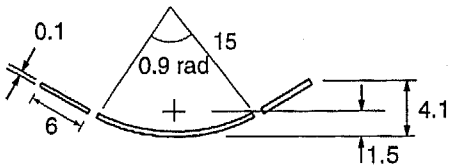

Fig. 8 Cross-section of 1" Sears tape spring (lengths in mm)

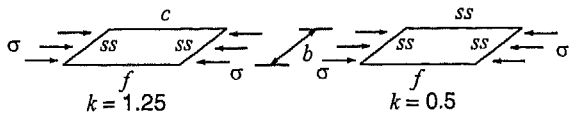

Fig. 9 Values of k for flat plates subject to different boundary conditions (c, clamped; f, free; ss, simply supported), from reference [18]

moment of area about the minor axis is $I = 4.67\,\text{mm}^4$ and the cross-sectional area is $A = 2.55\,\text{mm}^2$ [17].

Two different values of k have been considered: 1.25 and 0.5 (Fig. 9). The smallest value for b is the width of the flat edge of the cross-section, 6 mm, and the maximum value is half the arc-length, 12.7 mm. The flat edge has a simply supported edge and therefore $k = 0.5$, whereas, by symmetry the half arc-length can be assumed to be clamped and hence $k = 1.25$. Substituting these values into equation (7) gives a minimum value of $\sigma_{cr1} = 14.7\,\text{N/mm}^2$ and a maximum value of $\sigma_{cr1} = 26.4\,\text{N/mm}^2$. The value of $26.4\,\text{N/mm}^2$ is in good agreement with the experimental data and was therefore used.

Substituting the values of t and r for the tape spring, equation (8) gives $\sigma_{cr2} = 840\,\text{N/mm}^2$. Substituting this value into equation (11) gives

$$F_{cr}\left(\frac{1}{2.55} + \frac{e^2}{4.67\cos\sqrt{F_{cr}S^2/(4 \times 210\,000 \times 4.67)}}\right) = 840 \tag{13}$$

This equation has been solved numerically using MATLAB. The same method was also used to calculate the load that causes critical buckling at point 1. These two values of F_{cr} are then compared with the Euler buckling load and the lowest value is taken. F_{cr} was found to be 14.3 N.

Figure 10 shows the numerical predictions along with the experimental results. Note that the experimental results have been adjusted to take the self weight of the structure into account.

As can be seen in Fig. 10, the theoretical results match the experimental ones quite well. The exception is in the regions just after one of the tape springs has buckled. Here, only one side of the tape spring has buckled, and the tape spring is, therefore, in a transitional stage between being unbuckled and fully buckled. What is accurately modelled is the peak values and the very low stiffness in between the peak values.

5 PARAMETRIC DESIGN STUDY

Having developed a theoretical model for the force–displacement characteristics of the bistable structural element, the model can be used to formulate a design methodology. Typically, the design requirements will

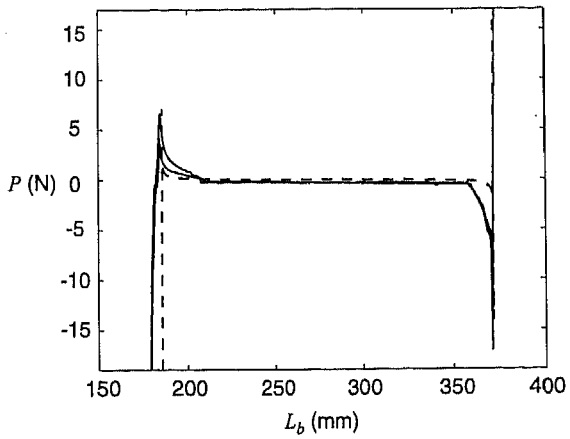

Fig. 10 Graph of P versus L_b: experimental results (solid line) and theoretical predictions (dashed)

provide the values of $P^{max}, P^{min}, L_b^{max}$, and L_b^{min}. The design variables in the structure include the material used for the tape springs, their cross-sectional areas, A_a and A_b, and their second moment of areas, I_a and I_b; in addition, the number of tape springs that connect opposite corners of the linkage, n_a and n_b, could be greater than one (forming a set of overlapping tape springs connected only at the ends) to achieve a greater force output. Also, the initial offsets of the tape springs, e_a and e_b, can be varied, as can the length of the tape springs, S_a and S_b, and the length of the bars, B. Given the large number of variables (11) and the number of user-defined parameters (4), it is not possible to set up a sufficient number of equations to determine the values of all the variables by solving a set of constraint equations.

In order to simplify matters, the following assumptions were made. The values of A and I were set equal to the values of the 1" Sears carpenter's tape. B was set arbitrarily equal to $(\sqrt{5}/4)L_b^{max}$. Finally, n_a and n_b were set to the minimum value possible in order to achieve the required forces. With these additional constraints, it is possible to calculate e_a, e_b, S_a, S_b, n_a, and n_b for given values of $P^{max}, P^{min}, L_b^{max}$, and L_b^{min}.

Finally, the variation of P^{max} and P^{min} with e_a and e_b was calculated. Figure 11 shows the results for the case $S_a = S_b = 372\,\text{mm}$.

As can be seen from Fig. 11, it is possible to achieve specified values of P^{max} and P^{min} quite accurately by varying e_a and e_b. If a high value of P is required, a positive value of e should be used. If the desired value of F is too low for an acceptably low (positive) value of e to be used, a negative value of e should be used instead. In practice, having a positive value of e would require that the tape spring be turned around in the structure in order to ensure that the two tape springs do not interfere with each other.

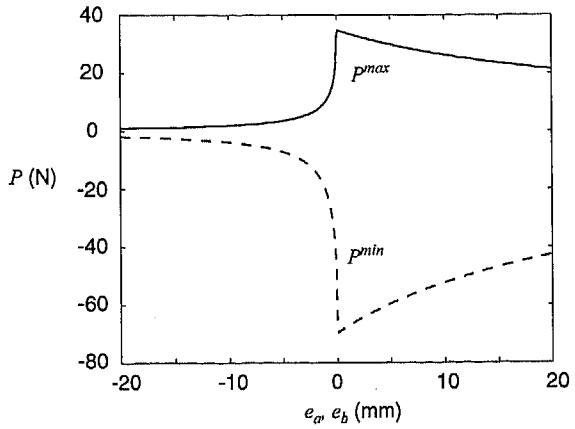

Fig. 11 Design graph for structural element with $B = 372$ mm long bars and one tape spring along each diagonal ($n_a = n_b = 1$)

6 DISCUSSION AND CONCLUSION

The bistable structural element proposed in this article has been modelled with good accuracy. The main discrepancies can be attributed to friction in the hinges, imperfections in the tape springs, and inaccuracies in the values of e_a and e_b.

A key advantage of the proposed concept is that its structural members carry loads mainly in compression or tension, thus minimizing bending effects. This feature makes the proposed design structurally efficient.

Two potential disadvantages of the particular implementation shown in Fig. 3 are that it requires mechanical hinges and that the tape springs buckle out of the plane of the linkage, which increases the potential for interference with other structural members.

The hinges can be replaced with 'living hinges' made out of thin polymer elements [21, 22]; these hinges are commonly found in consumer plastic goods. Figure 12 shows a second prototype of the proposed bistable element, with the tape springs rearranged in the plane of the structure and incorporating living hinges.

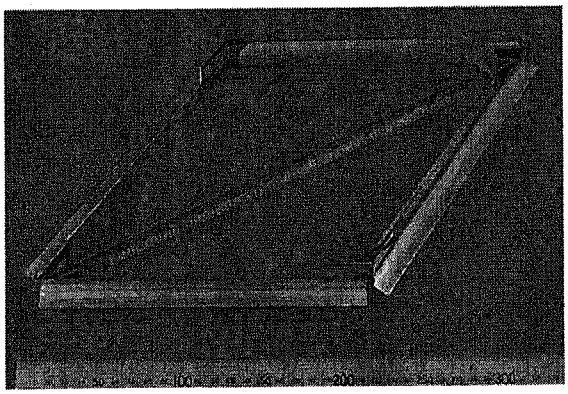

Fig. 12 Second prototype

ACKNOWLEDGEMENTS

The research presented in this article was carried out in the Department of Engineering, University of Cambridge, with funding from the Cambridge-MIT Institute and in collaboration with Professor Steve Dubowsky at MIT. Support from EPSRC in the form of a research studentship for T. S. is gratefully acknowledged.

REFERENCES

1 **Miura, K.** Variable geometry truss concept. Report 614, The Institute of Space and Astronautical Science, 1984.
2 **Rhodes, M.** and **Mikulas, M. M.** Deployable controllable geometry truss beam. NASA Technical Memorandum 86366, 1985.
3 **Miura, K., Furuya, H.,** and **Suzuki, K.** Variable geometry truss and its application to deployable truss and space crane arm. *Acta Astronaut.*, 1985, **12**, 599–607.
4 **Chen, G. S.** and **Wada, B. K.** Adaptive truss manipulator space crane concept. *J. Spacecr. Rockets*, 1993, **30**(1), 111–115.
5 **Pellegrino, S.** and **Calladine, C. R.** Matrix analysis of statically and kinematically indeterminate frameworks. *Int. J. Solids Struct.*, 1986, **22**, 409–428.
6 **Schioler, T.** and **Pellegrino, S.** Space frames with multiple stable configurations. *AIAA J.*, 2007, **45**, 1740–1747.
7 **Pieper, D. L.** *The kinematics of manipulators under computer control.* PhD Thesis, Stanford University, 1968.
8 **Chirikjian, G. S.** A binary paradigm for robotic manipulators. In Proceedings of the IEEE International Conference on *Robotics and Automation*, 1994, vol. 4, pp. 3063–3069.
9 **Chirikjian, G. S.** and **Burdick, J. W.** Kinematically optimal hyper-redundant manipulator configurations. *IEEE Trans. Robot. Autom.*, 1995, **11**(6), 794–806.
10 **Lees, D.** and **Chirikjian, G. S.** A combinatorial approach to trajectory planning for binary manipulators. In Proceedings of the IEEE International Conference on *Robotics and Automation*, April 1996, vol. 3, pp. 2749–2754.
11 **Lichter, M.** *Concept development for lightweight binary-actuated robotic devices, with application to space systems.* Master's Thesis, Massachusetts Institute of Technology, 2001.
12 **Wingert, A., Lichter, M., Dubowsky, S.,** and **Hafez, M.** Hyper-redundant robot manipulators actuated by optimized binary dielectric polymers. *Proc. SPIE*, 2002, **4695**, 415–423.
13 **Stuhakorn, J.** and **Chirikjian, G. S.** A new inverse kinematics algorithm for binary manipulators with many actuators. *Adv. Robot.*, 2001, **15**(2), 225–244.
14 **Plante, J.-S., Santer, M. J., Dubowsky, S.,** and **Pellegrino, S.** Compliant bistable dielectric elastomer actuators for binary mechatronic systems. In

Proceedings of the IDECT/CIE 2005: ASME Mechanism and Robotics Conference, Long Beach, CA, 24–28 September 2005 (ASME).
15 **Seffen, K. A.** and **Pellegrino, S.** Deployment dynamics of tape springs. *Proc. R. Soc. Lond. Ser. A*, 1999, **455** (1983), 1003–1048.
16 **Calladine, C. R.** The theory of thin shell structures 1888–1988. *Proc. Instn Mech. Engrs*, 1988, **202**, 1–9.
17 **Watt, A.** *Deployable structures with self-locking hinges.* PhD Thesis, Cambridge University, 2003.
18 **Allen, H. G.** and **Bulson, P. S.** *Background to buckling*, 1980 (McGraw-Hill, London).
19 **Timoshenko, S. P.** and **Gere, J. H.** *Theory of elastic stability* 1961 (McGraw-Hill, New York).
20 **Bazant, Z. P.** and **Cedolin, L.** *Stability of structures*, 1991 (Oxford University Press, Oxford).
21 **Tres, P. A.** *Designing plastic parts for assembly*, 2000 (Hanser Gardner Publications, Cincinnati).
22 **Howell, L. L.** *Compliant mechanisms*, 2001 (John Wiley & Sons, Inc., New York).

APPENDIX

Notation

a	moment arm for applied force
A	cross-sectional area of the tape spring
b	width of the rectangular plate
B	length of bars
c	distance from the centroid of the tape spring to the outer edge
e	eccentricity of axial loading of a column
E	Young's modulus
F	end force on tape spring
I	second moment of area
k	force-stiffness parameter
L_a	width of the structural element
L_b	length of the structural element
M_-^*	constant moment applied by buckled tape spring bent in an equal sense
M_+^*	constant moment applied by buckled tape spring bent in an opposite sense
n	integer parameter
P	force on the structural element
P_{cr}	critical (buckling) load of a column
P_E	Euler buckling load of a column
r	transverse radius of curvature of a tape spring
R	radius of curvature
S	length of the tape spring
t	thickness of the tape spring
w	central deflection of an eccentrically loaded tape spring
y	distance from centroid
α	angle subtended by the cross-section of a tape spring
θ	half-angle between bars of the four-bar linkage
ν	Poisson's ratio
σ	stress
σ_{cr}	buckling stress
ϕ	angle between the tape spring and the plane of four-bar linkage

Subscripts

a, b	two sets of tape springs